# Universal Analytical Modeling of the Optical Properties for Coated Plasmonic Nanoparticles

**Nikolai Khlebtsov[1,2*] and Sergey Zarkov[1,3]**

[1] Institute of Biochemistry and Physiology of Plants and Microorganisms, "Saratov Scientific Centre of the Russian Academy of Sciences," 13 Entuziastov pr., Saratov 410049, Russian Federation

[2] Saratov State University, 83 Astrakhanskaya str., Saratov 410012, Russian Federation

[3] Institute of Precision Mechanics and Control, "Saratov Scientific Centre of the Russian Academy of Sciences," 24 Rabochaya str., Saratov 410028, Russian Federation

*e-mail: khlebtsov@ibppm.ru

**Abstract.** We describe a new analytical method for coated plasmonic nanoparticles, combining the modal expansion method (MEM) with the dipole equivalence method (DEM). The universality and accuracy of our approach are demonstrated through comparisons of extinction and scattering spectra for variously shaped two-layer gold and silver nanoparticles (rods, disks, triangle prisms, bicones, and bipyramids) with dielectric coatings from 0 to 100 nm, benchmarked against numerical calculations using COMSOL. Due to its universality, the MEM + DEM approach accurately reproduces the dependence of extinction and scattering spectra on particle size, shape, shell thickness, and orientation relative to the incident light polarization. We also investigate the effects of size-corrected dielectric functions for gold and silver, along with related damping mechanisms, on the spectra. As expected, size-dependent damping broadens and reduces plasmonic peaks, especially for small silver nanoparticles. Although MEM inherently does not depend on particle shape, the MEM + DEM method fails for coated bicones with sharp tips but performs satisfactorily for rounded bicones. This limitation is due to strong localization of plasmonic fields near the tips, which violates the assumption of homogeneous internal fields and the applicability of DEM. To avoid this difficulty, we introduce a factorized version of MEM that ensures accurate analytical calculations for coated sharp bicones. In summary, the MEM + DEM approach provides a simple yet accurate analytical tool for simulating various plasmonic properties of coated metal nanoparticles and for developing machine learning models.

**Keywords:** gold and silver nanoparticles; coated nanoparticles, localized plasmon resonance; modal expansion method; dipole equivalence method; COMSOL.

Paper #9423 received 7 Nov 2025; revised manuscript received 4 Dec 2025; accepted for publication 5 Dec 2025; published online 23 Dec 2025. doi: 10.18287/JBPE25.11.040306.

## 1 Introduction

Biomedical applications of plasmonic nanoparticle conjugates require functionalization of their surface with various functional molecules, which ensure their stability in the bloodstream, invisibility for immune system cells, targeting specific biotarget sites, etc. [1−23]. Often, such properties are achieved in hybrid multilayer structures with silica-type dielectric shells. Thus, from a structural point of view, multifunctional bioconjugates are at least bilayer particles with a metal core and a dielectric coating. The optical properties of such conjugates differ from those of the plasmonic core and, in principle, can be simulated by modern numerical methods, such as the finite element method [4], the boundary element method [5, 6], the finite difference time domain method [7], and the discrete dipole approximation [8]. For applications of these methods to specific plasmonic problems and comparison of their efficiency the readers are referred to recent reviews [9, 10]. However, analytical models based on simple physical ideas are more in demand to control the various stages of synthesis in situ to predict given optical properties and their

correlation with the structure of particles. Besides, analytical methods can be useful in application of AI tools based on deep machine learning models.

In this paper, we describe an analytical model of this type [11], which is based on a combination of two methods: the modal expansion method (MEM) [12] and the dipole equivalence method (DEM) [13]. The main advantage of the DEM method is that the analytical MEM models for particles of various shapes are also applicable for particles with a single-layer or even multilayer dielectric coating. In this communication, the capabilities of our method are illustrated by comparing analytical and numerical (COMSOL) extinction and scattering spectra of gold and silver nanorods (NRs), nanodiscs (NDs), triangular nanoprisms (NTs), bicones (BCs), and bipyramids (BPs).

In our previous papers [11, 14] we used the bulk dielectric functions of silver and gold. Here, we extend our consideration to include the effects of size-corrected dielectric function caused by limitation of the mean free path of conductive electrons. The history of this point dates back to pioneering works by Doyle [15], Hampe [16], and Fragstein and Römer [17] published in 1958. Doyle discovered that the plasmon resonance widths (0.05–0.5 eV) of NaCl crystals did not match the calculated bulk value of 0.02 eV. He suggested that this anomaly could be explained by the limitation of the electron mean free path, which cannot be larger than the nanoparticle size. Therefore, the classical electron mean free path (~20 nm) should be replaced with the actual size of the NaCl particles. Similarly, Hampe observed significant broadening of the absorption spectra of gold nanoparticles in a silicate matrix and proposed that this could also be explained by the limitation of the electron mean free path. Römer and Fragstein [18] measured the refractive index of gold nanoparticles ranging from 3 to 20 nm and found significant differences between the optical constants of bulk gold and those measured for the smallest 3.5 nm particles. Consistent with Doyle [15] and Hampe [16], they speculated that these anomalies might be related to size-correction effects. In 1969, Kreibig and Fragstein [19] developed a comprehensive classical model of the size-corrected dielectric function in metal nanoparticles, incorporating the size-dependent damping constant $\gamma_p(a)$

$$\gamma_p(a) = \gamma_b + \gamma_s = \gamma_b + A_s \frac{v_F}{a}, \qquad (1)$$

where $\gamma_b$ is the dumping constant of bulk metal, $v_F$ is the Fermi velocity, $a$ is the radius of a spherical nanoparticle, and the scattering constant $A_s$ depends on the scattering model of conductive electrons at the particle surface. The modified dumping constant $\gamma(a)$ should be substituted into the classical Drude-Lorentz [20] theory for the dielectric function of conductive electrons. Since the publication of these early works, the size-corrected dielectric function, based on the modified dumping constant (Eq. (1)) within the Drude-Lorentz theory, has been widely used in many studies [21−26].

In line with many previous studies [26, 27], we demonstrate that size-dependent dumping results in broadening and reduction of the plasmonic peaks of coated nanoparticles, especially for small silver nanoparticles. For the main localized plasmon resonance (LPR) peaks, the analytical method accurately describes the changes in extinction and scattering spectra with increasing dielectric shell thickness for all particle types. However, we observed noticeable differences between the analytical spectra and their numerical counterparts for bicones and bipyramids. These differences are due to strong near-field localization near sharp vertices, which violates the conditions for applying the dipole approximation. To improve the original MEM + DEM scheme, we propose a factorized MEM model where the effective path length is adjusted via an additional MEM parameter that depends on the dielectric coating thickness. This correction is shape- and size-independent, making it broadly applicable.

## 2 Methods and Materials

Our MEM models are similar to those previously described [11], with differences in parametrization and size-dependent corrections for the dielectric constants of gold and silver. Figure 1 shows the five particle shapes considered in this work. We also define the geometrical parameters in terms of the characteristic particle size $L$ and a generalized aspect ratio $AR$. Panel B illustrates the parametrization of coated nanorods. The particle core is characterized by a complex permittivity $\varepsilon_1$, while a homogeneous shell is described by its thickness $s$, and permittivity $\varepsilon_2 = 2.25$, which corresponds to a typical refractive index of 1.5 for most stabilizing ligands and functional coatings [28]. The surrounding medium is characterized by its dielectric function $\varepsilon_m$, (water in this work).

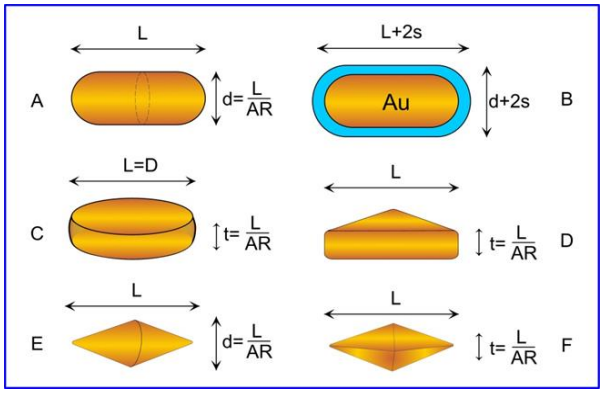


Fig. 1 The characteristic length $L$ and a generalized aspect ratio $AR$ characterize geometrical models for five particle morphologies. Panel B illustrates NP coating with a dielectric shell of constant thickness $s$; (A) NRs have hemispherical caps at the tips; (C) nanodisks have semicircular edge profile; (D) nanotriangle prisms have smooth edges with rounding radius $(L + t) / 40$; (E) bicones have rounded tips and circular base edge with rounding radii $d / 40$ and $d / 100$, respectively; (F) bipyramids have the pentagonal base and smooth tips edges.

To eliminate sharp edges for prisms and bipyramids, we used small smoothing parameters proposed by Yu et al. [12]. However, the experimental as-prepared and chemically etched bipyramids have variable tip and base radii, which are significantly larger than those in rounding model by Yu et al. [12]. Specifically, the radii of the tips and base increase as the overall length of the bipyramid decreases [29]. Since the bipyramid diameter remains nearly constant during chemical etching, the experimental data can be approximated by simple linear relationships.

$$R_{tip}(\text{nm}) = 14 - 2AR_1,$$
$$R_{base}(\text{nm}) = 16 - 2AR_1, \quad (2)$$
$$AR_1 \le 6.$$

For benchmark calculations, we use the finite element method with the commercial package COMSOL Multiphysics 5.1 (Wave Optics module) and T-matrix codes [30]. For details concerning COMSOL and T-matrix simulations as well as the tabulated optical constants data and its approximations, the readers are referred to our previous works [11, 14].

To calculate the size-corrected dielectric functions of gold and silver we used the classical approach [19, 26, 27] in which the tabulated bulk data arte corrected by difference between the Drude-Lorentz conductive electron terms with bulk and size-corrected dumping constants

$$\Delta\varepsilon(\omega, a) = \frac{\omega_p^2}{\omega(\omega + i\gamma_b)} - \frac{\omega_p^2}{\omega(\omega + i\gamma_p)}. \quad (3)$$

In Eq. (3), the particle dumping parameter $\gamma_p$ is given by Eq. (1) with the scattering constant $A_s$ which includes two contributions from the surface electron scattering [19] and the chemical interface dumping chemical interface damping (CID) caused by changing the nanoparticle's chemical interface [31, 32]

$$\gamma_s = \left(A_s^{surf} + A_s^{CID}\right)\frac{v_F}{l_s} = A_s\frac{v_F}{l_s}, \quad (4)$$

where the mean free path of electrons $l_s$ is proportional to the ratio of the particle volume $V$ and surface $S$ according to the Coronado and Schatz [33] Eq.:

$$l_s = \frac{4V}{S}. \quad (5)$$

Note that we did not include radiation dumping term [34, 35] in Eq. (4) because the full wave finite element method (FEM) solution accounts for the radiation dumping automatically.

One important note concerning possible quantum mechanical (QM) effects in small metal particles is in order. Kawabata and Kubo [36] were the first to note that the classical interpretation of size effects, based on surface electron scattering by the nanoparticle surface, is not correct. According to QM treatment, the size-correction effect stems from the appearance of surface discrete levels and an additional imaginary part of the dielectric function due to dipole transitions between these levels. However, it was an unexpected result that more sophisticated QM calculations led to the same inverse proportionality between the damping constant and the characteristic particle size [37−39]. Therefore, here we adopt the classical size-correction scheme (Eqs. (3−5)).

In our MEM + DEM method [11], the generalized polarizability of a coated plasmonic particle is given by the following analytical expression:

$$\alpha_{av} = R_{2ev}^3 \sum_j q_j(h_2)\frac{\bar{\varepsilon}_j - \varepsilon_m}{3\varepsilon_m + 3L_{2mj}(\bar{\varepsilon}_j - \varepsilon_m)}, \quad (6)$$

$$L_{2mj} = \frac{1}{1-\eta_j(h_2)} - A_j(h_2, \varepsilon_m), \quad (7)$$

$$A_j(h_2, \varepsilon_m) = a_{j2}(h_2)x_{2m}^2 + i\frac{2}{9}q_j(h_2)X_{2m}^3 + a_{j4}(h_2)x_{2m}^4, \quad (8)$$

$$x_{2m} = \frac{L_2 k_m}{2\pi},\ X_{2m} = R_{2ev}k_m,\ k_m = k\sqrt{\varepsilon_m}, \quad (9)$$

where the summation is over all modes "$j$" ($j = 1$ corresponds to the dipole eigenmode); $R_{2ev}$ and $L_2$ are the equivolume sphere radius of the coated particle and its characteristic size, respectively, $q_j(h_2) = V_j^m(h_2)/V_2$ are the modal volume fractions for mode "$j$", $V_j^m(h_2)$ and $V_2$ are the modal and total volumes of the coated particle. For metal particles without coating, the parameter $\bar{\varepsilon}_j$ is simply replaced by the metal dielectric function $\varepsilon_1$ reducing the above equations to the original MEM form [12]. Eigenvalues $\eta_j(h_1)$ and $\eta_j(h_2)$ are the key parameters of MEM. They depend on the particle shape only or, in other words, on the generalized aspect ratio $h_i = AR_i$, $i = 1, 2$. It should be emphasized here that $\eta_j(h_1)$ and $\eta_j(h_2)$ do not depend on the particle size, composition, or environment thus making MEM + DEM approach quite universal. Analytical expressions for all MEM parameters are available in our previous work [11].

The MEM polarizability (Eq. (6)) depends on the incident light's polarization but not on its direction relative to the particle frame. In practice, the extinction and scattering cross sections averaged over random particle orientations are given by following Eqs. [30]:

$$\langle C_{ext}\rangle = \pi R_2^2\langle Q_{ext}\rangle = \frac{4\pi}{k_m'}\text{Im}\left(k_m^2\frac{\alpha_{av}^x + \alpha_{av}^y + \alpha_{av}^z}{3}\right), \quad (10)$$

$$\langle C_{sca}\rangle = \pi R_2^2\langle Q_{sca}\rangle = \frac{8\pi}{3}|k_m|^4\frac{|\alpha_{av}^x|^2 + |\alpha_{av}^y|^2 + |\alpha_{av}^z|^2}{3}, \quad (11)$$

where $k_m' = \text{Re}(k_m) = (2\pi/\lambda)\text{Re}(n_m)$, is the real part of the wave vector modulus, the angular brackets stand for averaging over random orientations, and superscripts *x*, *y*, *z* correspond to polarizations of the incident light along the frame axes related to the particle.

## 3 Results and Discussion

First, consider the effects of dielectric coating on plasmonic cores with bulk optical constants. Figure 2 shows the excellent accuracy of the analytical model in predicting the main LPR peaks for randomly oriented silver and gold nanorods as the shell thickness increases from 0 to 30 nm. In this and subsequent figures, the shell refractive index is 1.5, and the external medium is water. A similar agreement between analytical and numerical spectra was observed for scattering cross sections (data not shown).

Extensive COMSOL and MEM + DEM simulations show that the analytical MEM + DEM approach accurately predicts the extinction and scattering spectra of gold and silver nanorods with a maximum length of 200 nm, aspect ratios from 1 to 6, and dielectric shell thicknesses up to 100 nm.

The greatest difference between COM and MEM solutions for gold nanorods occurs at a moderate aspect ratio ($AR$ = 2) and a maximum shell thickness of 30 nm. The COM model gives extinction and scattering peaks of $C_e$ = 1379 nm$^2$ and $C_s$ = 73.9 nm$^2$ at 646 nm, compared to MEM values of 1359 nm$^2$ and 64 nm$^2$ at 642 nm. This results in maximal errors of approximately 0.6% in peak position and 1.5% in extinction cross section. The error for the scattering resonance peak is significantly larger, about 14%. These trends are similar for silver nanorods. It is important to note that all comparisons between MEM and COMSOL focus only on the main dipolar plasmonic peaks, as MEM does not capture minor multipolar extinction and scattering peaks.

Figure 3 compares numerical (blue) and analytical (red) extinction (A) and scattering (B) spectra calculated for in-plane excitation of silver disks with the coating thicknesses from 0 to 30 nm. Minor short wavelength peaks are omitted because MEM theory does not reproduce them. There is excellent agreement between analytical and numerical spectra in peak positions, amplitudes, and their dependence on the shell coating thickness. Based on extensive simulations, the analytical approach is valid for gold and silver disks with a core diameter of 120 nm, core thickness of 20 nm, and shell thickness of 60 nm. The above numbers should be considered upper boundaries. The maximal MEM errors for gold NDs occur for 20 × 120 nm disks with a 30-nm coating. In particular, the PR peak positions and the extinction and scattering cross sections are: MEM – 787 nm, $1.281 \times 10^5$ nm$^2$, and $1.092 \times 10^5$ nm$^2$, respectively; COM – 784 nm, $1.281 \times 10^5$ nm$^2$, and $1.092 \times 10^5$ nm$^2$, respectively. For silver NDs similar numbers are: 787 nm, $1.348 \times 10^5$ nm$^2$, and $1.046 \times 10^5$ nm$^2$, respectively. Thus, the corresponding relative MEM errors are 0.4%, 0%, and 4.4%. For AgNDs, similar estimations give a bit higher errors: 1% (peak position), 3.2% (extinction peak), and 1.2% (scattering peak).

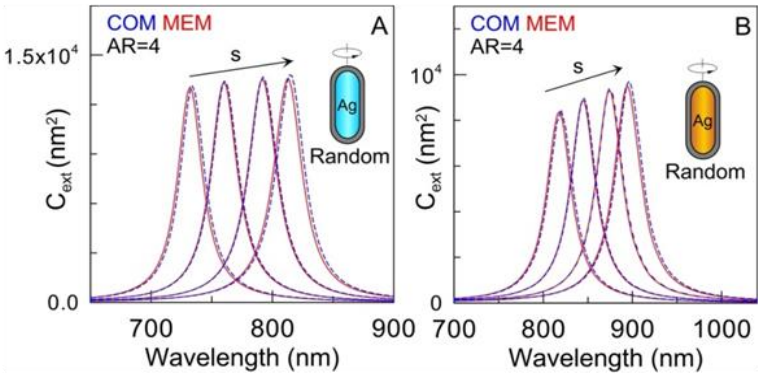


Fig. 2 (A) Extinction spectra of randomly oriented silver and (B) gold coated nanorods with a core diameter of 15 nm, aspect ratio 4, and coating thicknesses s = 0, 3, 10, and 30 nm. Calculations by COMSOL (blue) and MEM + DEM (red) methods.

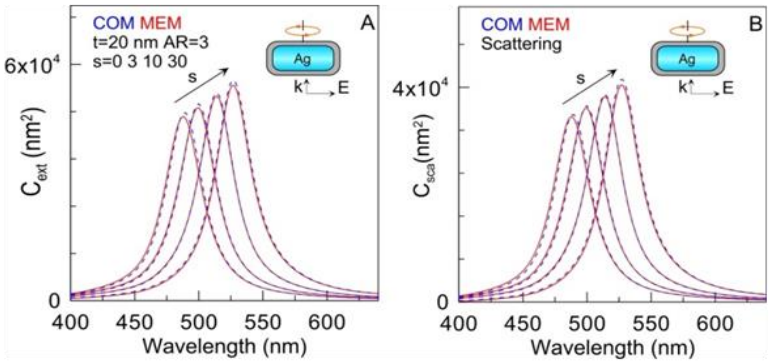


Fig. 3 (A) Extinction and (B) scattering spectra of silver nanodisks at in-plane excitation. The coating thicknesses s = 0, 3, 10, and 30 nm, and the disk thickness and aspect ratio are 20 nm and 3, respectively. Calculations by COMSOL (blue) and MEM + DEM (red) methods.

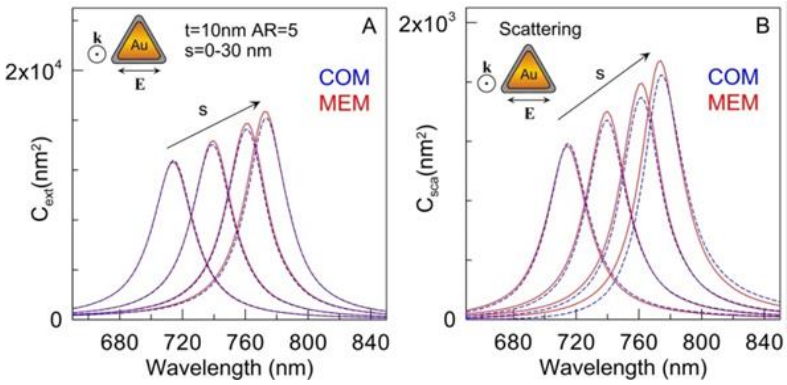


Fig. 4 (A) Extinction and (B) scattering spectra of gold nanotriangles with a thickness of 10 nm and aspect ratio of 5. Note that the scattering cross-section values are one order less than those for the extinction cross sections.

Figure 4 demonstrates the excellent accuracy of the analytical MEM + DEM method in predicting the extinction and scattering spectra of gold triangular nanoprisms with a 10 nm thickness and increasing dielectric coating from 0 to 30 nm. Similar results were obtained for silver and gold nanotriangles of various thicknesses. Minor short-wavelength multipolar peaks from COMSOL are not shown here. For gold NTs, most significant difference between MEM and COM spectra peaks occur for a thick $30 \times 150$-nm particles without coating: MEM – 810 nm, $1.345 \times 10^5$ nm$^2$, and $1.030 \times 10^5$ nm$^2$, respectively; COM – 814 nm, $1.425 \times 10^5$ nm$^2$, and $1.102 \times 10^5$ nm$^2$, respectively. In other words, the percentage differences are 0.5% (peak position), 5.6% (extinction), and 6.5% (scattering). Finally, for bare $30 \times 250$ nm silver NTs, the percentage difference between MEM and COM peak position, extinction and scattering are 0.8%, 5.3%, and 5.45%, respectively.

Compared to rods, disks, and triangles, the analytical spectra of coated bicones and bipyramids did not match the numerical results obtained with COMSOL. We investigated this issue and hypothesize that the discrepancy between MEM + DEM and COMSOL may be due to strong localization of the local field near the sharp bicone tips [11]. We also compared the COMSOL and MEM dependencies of plasmonic peak positions on shell thickness, starting with very thin coatings of 0.2 nm. These dependencies differ significantly when plotted against both shell thickness and shell volume fraction. Specifically, COMSOL predicts larger plasmonic shifts than MEM. One possible explanation is the concept of the local shell volume fraction excited by the intense local field near the bicone tips. This feature enhances the sensitivity of plasmonic bicones and bipyramids [40] to their local environment. However, the strong localization near the tips violates the assumption of a homogeneous internal field distribution, which questions the physical basis of MEM + DEM in this context.

To improve the MEM accuracy, we introduced [11] a new MEM + DEM version in which the MEM parameter $\varepsilon_1(AR)$ and the modal volume function $V_1(AR)$ are represented in factorized forms $\varepsilon_1(AR)\, f_\varepsilon(s)$ and $V_1(AR)\, f_V(s)$ where functions $f_\varepsilon(s)$ and $f_V(s)$ depend on the shell thickness only and do not depend on the particle metal, size, and shape. In the original version of MEM [12], the modal volumes and eigenvalues were functions only of the generalized shape parameter and did not depend on the particle size or their material (gold or silver). Our proposed theory for coated plasmonic particles [11] used the dipole equivalence method we developed earlier [13] to relate the original MEM polarizability of a metal particle to the polarizability of a coated particle. Generally speaking, it was not obvious a priori that this approach would work for particles of arbitrary shape. However, comparison with numerical calculations showed that for all realistic particle models, including pentagonal bipyramids with vertex radii of 2−6 nm, the MEM + DEM method yields excellent results. An exception was found only for a model with a geometric feature – a bicone with a very small vertex radius of curvature. For this model, the influence of a very thin coating exhibits clear nonlinearity, and the analytical spectra disagree with the numerical ones regarding the coating-induced shift of the plasmon resonance. As we stated previously, the physical reason for this is related to the strong non-uniformity of the local field near the vertices. From a physical point of view, this means that the modal volumes and eigenvalues of the electrostatic problem should now depend not only on the shape but also on the coating thickness. In the general case, they should be functions of two variables. The idea of the factorization method is that these (unknown) functions of two variables can be represented as a product of shape functions and coating thickness functions. Here, the shape functions are the same universal parameters of the original MEM and do not depend on the particle size or shape material. On the other hand, the coating thickness functions should be equal to 1 at zero thickness. They also do not depend on the particle size and, to a first approximation, do not depend on the shape material.

We derived the factorized functions by comparing benchmark simulations with analytical spectra and introduced them to the calculation scheme. Figure 5 illustrates the excellent accuracy of the factorized MEM method in predicting the extinction and scattering cross-section spectra. Similar results were obtained for coated

gold and silver bicones with other aspect ratios from 2 to 6 and other diameters from 10 to 30 nm. Note that because of more complex factorized MEM+DEM parametrization, we used different MEM parameters for silver and gold bipyramids. In a sense, the universality of the factorized analytical method is somewhat limited, but this is compensated by higher accuracy.

By contrast to sharp-tipped bicones, for bipyramids with the rounding radii as given by Eq. (2) the MEM + DEM analytical method works almost perfectly without any additional factorized parametrization for the eigenvalues and modal volumes (Fig. 6). Figure 6 demonstrates excellent accuracy of MEM + DEM method for extinction spectra of gold and silver bipyramids with dielectric coating thickness ranging from zero (bare metal) to 30 nm. In this simulations, the width of bipyramids was set to be 30 nm and the aspect ratio varied from 2 to 5, in agreement with most experimental observations [29, 41−44]. The shell thickness was varied from 0 to 30 nm although equally good agreement between MEM and COMSOL spectra was obtained for thicker shells (up to 60 nm) when the shell volume fraction was greater than 0.9. The main differences between MEM and COM spectra are observed for slightly elongated ($AR$ = 2) coated ($s$ = 30 nm) gold bipyramids. For example, the peak positions and amplitudes are: MEM – 564 nm, 4649 nm$^2$ (extinction), and 316 nm$^2$ (scattering); COM – 568 nm, 4832 nm$^2$ (extinction), and 365 nm$^2$ (scattering). Accordingly, the percentage difference between MEM and COM peak position, extinction and scattering are 0.7%, 3.8%, and 13.4%, respectively. Similar estimations hold also for silver bipyramids.

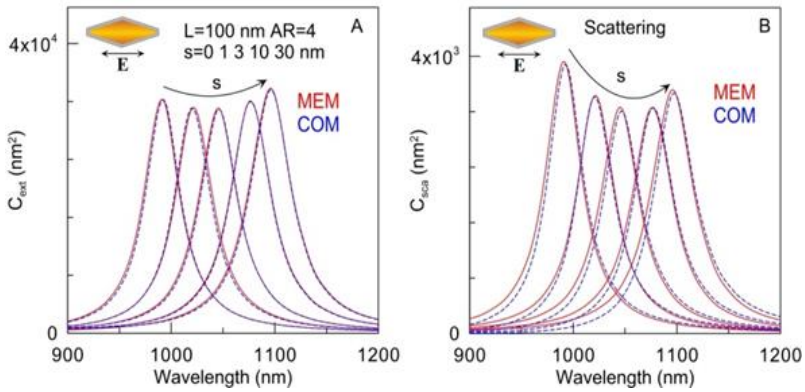


Fig. 5 Extinction (A) and scattering (B) spectra coated gold bicones excited along the symmetry axis $L$=100 nm. The aspect ratio is 4, and the coating thicknesses are s=0, 1, 3, 10, and 30 nm. Calculations by COMSOL (blue) and factorized MEM + DEM (red) methods. Note the extraordinary sensitivity of the LPR peak position to the local environment (thin 1-nm dielectric coating).

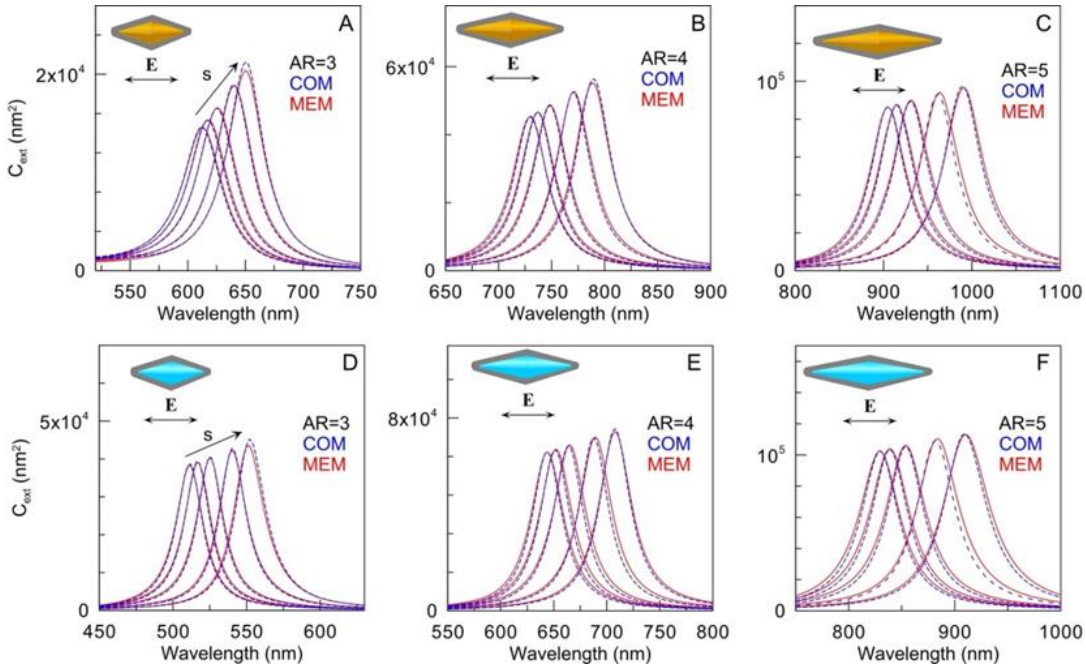


Fig. 6 Extinction spectra of gold (A-C) and silver (D-F) bipyramids calculated by MEM (red) and COMSOL (blue) for a constant width of 30 nm and aspect ratios 3, 4, and 5. The shell thicknesses are 0, 1, 3, 10, and 30 nm. The rounding radii are given by Eq. (2).

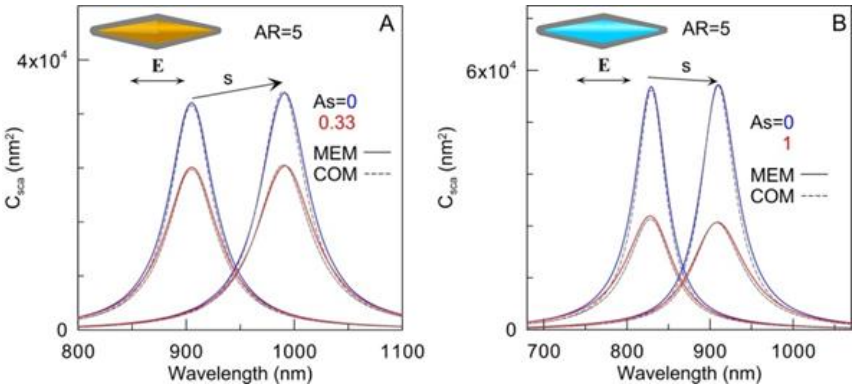


Fig. 7 Scattering spectra of (A) gold and (B) silver bare and coated ($s$ = 30 nm) bipyramids with a fixed diameter of 30 nm, aspect ratios of 5, and rounding radii of tips and bases are determined by Eq. (2). Calculations by COMSOL (dashed lines) and MEM (solid lines) under in longitudinal excitation for bulk ($A_s$ = 0, blue) and size-corrected optical constants ($A_s$ = 0.33 for gold and $A_s$ = 1 for silver, red).

Now, we briefly discuss the main differences between extinction and scattering spectra calculated using bulk and size-corrected optical constants for gold and silver (a more detailed discussion can be found elsewhere [45]). In practical simulations, selecting the electron scattering constant is the most challenging step. For literature data and discussion of this point, the readers are referred to papers [25, 26]. In this work, we used $A_s$ = 0.33 [46, 47] for gold and $A_s$ = 1 for silver [25]. We conducted extensive simulations for five particle models, two metals (gold and silver), and shell thicknesses ranging from 0 to 100 nm. These results will be discussed elsewhere. Here, we focus on a single example that exhibits the most pronounced size-correction effects.

Figure 7 shows scattering spectra of gold and silver bare ($s$ = 0) and coated ($s$ = 30 nm) bipyramids. Calculations were performed for bulk ($A_s$ = 0, blue) and size-corrected ($A_s$ = 0.33 for gold and 1 for silver; red) dielectric functions. First, we again note excellent agreement between analytical (MEM) and numerical (COMSOL) spectra. Second, there is significant reduction of resonance scattering amplitudes and peak broadening, especially for silver particles. Finally, we note somewhat unusual decrease in scattering peak for coated silver particles. Similar effects were described and explained previously [11].

## 4 Comparison of MEM + DEM with Other Analytical Approximations

The simplest analytical approach is the quasi-static (or electrostatic) approximation (EA), which is valid in the limit of small particle sizes. In particular, analytical solutions are known for two-layered spheres and spheroids [48]. However, we have previously shown [14] that for gold and silver spheroids with sizes on the order of 50−100 nm, the EA is not applicable for predicting either the position or the amplitude of the plasmon resonance, even for metallic particles, let alone coated ones.

Another physical approach is to treat a plasmonic particle with a single-layer or multi-layer dielectric coating as a homogeneous particle with some effective refractive index. Essentially, a similar idea underlies the Discrete Dipole Approximation (DEM). There are many theoretical approaches of this type, collectively known as the family of effective medium approximations (EMA) [49]. The history of EMA goes back to pioneering works by Maxwell Garnett [50] and Bruggeman [51], with sequential development in many reports (see, e.g., Refs. [52] and [53]). Stroud and Pan [54] suggested a so-called extended EMA (EEMA) to go beyond the small-size limitation of classical EMA. For a very useful and detailed discussion of various EMA versions, the reader is referred to the book chapter by Chylek et al. [49]. All versions of EMA are computationally simple and offer analytical insight into the averaged behavior of various composites. They can describe phenomena such as the plasmonic redshift with increasing filling fraction. However, they have serious limitations because the key assumption of EMA is that inclusions are small, typically spherical in shape, isolated, and embedded in a homogeneous local field. In other words, arbitrary particle shapes and sizes are beyond the typical EMA framework, which works within the small-sphere limit. In contrast, the MEM + DEM approach is designed for plasmonic coated particles of arbitrary shape and typical core sizes under 150 nm, offering reasonable accuracy compared to more time-consuming numerical methods.

The quasinormal mode (QNM) method is a more sophisticated semi-analytical approach for open resonant systems, such as optical cavities, nanoparticles, and metamolecules [55]. Quasinormal modes are the complex-frequency eigenmodes of such systems with radiative losses. Once the QNMs are computed (typically via a numerical solver like FEM or finite difference time domain (FDTD)), the optical properties are represented as a sum over QNMs. Such expansions provide an efficient and physically intuitive approach to describe Purcell effect and Fano resonances. However, the accuracy of the expansion depends on the completeness of the QNM set, which makes the QNM approach more complex and computationally demanding compared to MEM + DEM. For complex systems like large-scale random colloidal aggregates, QNMs become impractical.

## 5 Conclusion

We have expanded the MEM approximation developed for metallic nanoparticles to the coated nanostructures. It should be emphasized that our MEM + DEM approach does not require any additional numerical simulations except for those needed for the original MEM. By comparing analytical spectra with benchmark COMSOL simulations, we have demonstrated excellent accuracy and shape universality of the MEM + DEM approach.

Based on extensive simulations (the full data are not shown here; see, for instance, related references [11, 14, 45]) we can recommend the MEM + DEM approach for various coated particle geometries, provided that their maximal size, coating thickness, and generalized aspect ratio do not exceed 150 nm, 60 nm, and 10, respectively. Moreover, MEM + DEM is applicable to particles with either bulk or size-corrected optical constants [45]. Finally, their minimal curvature radii should be greater than those indicated in the original MEM paper [12]. For typical experimental pentagonal bipyramids, MEM + DEM is applicable as is.

We hope this extension can find valuable applications in simulating various properties of coated plasmonic particles. In particular, it would help us understand how the particle coating modulates absorption and scattering spectra, plasmon quantum yield, SERS enhancement, and metal-enhanced fluorescence. In particular, the MEM + DEM approach provides a simple yet accurate analytical tool for simulating the plasmonic properties of coated metal nanoparticles and for developing machine-learning models. Recent trends clearly indicate a significant growth in studies and publications that integrate state-of-the-art synthesis protocols with AI capabilities [56−60] Two instructive examples applying machine learning to the synthesis of gold nanorods [61] and nanostars [62] were recently published. The developed MEM + DEM analytical models are believed to be useful for predicting optimal strategies to achieve precise optical control of both intermediate and final nanoparticle products.

## Funding

This work was funded by the Ministry of Science and Higher Education of the Russian Federation as a state assignment for the Saratov Scientific Centre of the Russian Academy of Sciences (research topic no. 124020100134-6).

## Conflict of Interest

The authors declare that they have no known competing financial interests or personal relationships that could have appeared to influence the work reported in this paper.

## References

1. T. Patil, R. Gambhir, A. Vibhute, and A. P. Tiwari, “Gold nanoparticles: synthesis methods, functionalization and biological applications,” Journal of Cluster Science 34(2), 705–725 (2023).
2. J. W. Lee, S.-R. Choi, and J. H. Heo, “Simultaneous stabilization and functionalization of gold nanoparticles via biomolecule conjugation: progress and perspectives,” ACS Applied Materials & Interfaces Journal 13(36), 42311–42328 (2021).
3. W. A. Arcos Rosero, A. Bueno Barbezan, C. Daruich De Souza, and M. E. Chuery Martins Rostelato, “Review of advances in coating and functionalization of gold nanoparticles: from theory to biomedical application,” Pharmaceutics 16(2), 255 (2024).
4. J. Jin, The Finite Element Method in Electromagnetics, 2nd ed., Wiley, New York (2002).
5. N. Ida, Numerical Modeling for Electromagnetic Non-destructive evaluation, Springer Science & Business Media (1994).
6. F. J. García De Abajo, A. Howie, “Retarded field calculation of electron energy loss in inhomogeneous dielectrics,” Physical Review B 65(11), 115418 (2002).
7. A. Taflove, Computational Electrodynamics: the Finite-Difference Time-Domain Method, Artech House, Boston (1995).
8. M. A. Yurkin, “Discrete dipole approximation,” Light, Plasmonics and Particles, 167–198 (2023).
9. A. Amirjani. S. K. Sadrnezhaad, “Computational electromagnetics in plasmonic nanostructures,” Journal of Materials Chemistry C 9(31), 9791–9819 (2021).
10. Parsons, C. P. Burrows, J. R. Sambles, and W. L. Barnes, “A comparison of techniques used to simulate the scattering of electromagnetic radiation by metallic nanostructures,” Journal of Modern Optics 57(5), 356–365 (2010).
11. N. G. Khlebtsov, S. V. Zarkov, “Combining the modal expansion and dipole equivalence methods for coated plasmonic particles of various shapes,” The Journal of Physical Chemistry C 129(24), 10958–10974 (2025).
12. R. Yu, L. M. Liz-Marzán, and F. J. García De Abajo, “Universal analytical modeling of plasmonic nanoparticles,” Chemical Society Reviews 46(22), 6710–6724 (2017).
13. N. G. Khlebtsov, “T-matrix method in plasmonics: an overview,” Journal of Quantitative Spectroscopy and Radiative Transfer 123, 184–217 (2013).
14. N. G. Khlebtsov, S. V. Zarkov, “Analytical modeling of coated plasmonic particles,” The Journal of Physical Chemistry C 128, 15029−15040 (2024).

15. W. T. Doyle, "Absorption of light by colloids in alkali halide crystals," Physical Review 111(4), 1067–1072 (1958).
16. W. Hampe, "Beitrag zur deutung der anomalen optischen eigenschaften feinstteiliger metallkolloide in grofler konzentration. teil ii: experimentelle ermittlung der absorptionskurve und deutung des absorptionsmechanismus des systemes Gold-$SiO_2$," Zeitschrift für Physik 152, 476–494 (1958).
17. C. V. Fragstein, H. Römer, "Uber die anomalie der optischen konstanten," Zeitschrift für Physik 151, 54–71 (1958).
18. H. Römer, C. V. Fragstein, "Bestimmung des Absorptionskoeffizienten und des Brechungsquotienten von kolloidalem Gold: Ein Beitrag zur «Anomalie der optischen konstanten," Zeitschrift für Physik 163(1), 27–43 (1961).
19. U. Kreibig, C. V. Fragstein, "The limitation of electron mean free path in small silver particles," Zeitschrift für Physik 224(4), 307–323 (1969).
20. P. Drude, "Ueber die beziehung der dielectricitätsconstanten zum optischen brechungsexponenten," Annalen der Physik 284(3), 536–545 (1893).
21. R. H. Doremus, "Optical properties of small gold particles," The Journal of Chemical Physics 40(8), 2389–2396 (1964).
22. U. Kreibig, "Electronic properties of small silver particles: the optical constants and their temperature dependence," Journal of Physics F: Metal Physics 4(7), 999–1014 (1974).
23. C. G. Granqvist, O. Hunderi, "Optical properties of ultrafine gold particles," Physical Review B 16(8), 3513–3534 (1977).
24. N. G. Khlebtsov, V. A. Bogatyrev, L. A. Dykman, and A. G. Melnikov, "Spectral extinction of colloidal gold and its biospecific conjugates," Journal of Colloid and Interface Science 180(2), 436–445 (1996).
25. U. Kreibig, L. Genzel, "Optical absorption of small metallic particles," Surface Science 156, 678–700 (1985).
26. N. G. Khlebtsov, "Optics and biophotonics of nanoparticles with a plasmon resonance," Quantum Electronics 38(6), 504–529 (2008).
27. U. Kreibig, M. Vollmer, Optical properties of metal clusters, Springer Series in Materials Science, Springer Berlin, Heidelberg (1995). eBook ISBN: 978-3-662-09109-8.
28. L. Liz-Marzán, Colloidal synthesis of plasmonic nanometals, 1st ed., Jenny Stanford Publishing, 2020.
29. J. L. Montaño-Priede, A. Sánchez-Iglesias, S. A. Mezzasalma, J. Sancho-Parramon, and M. Grzelczak, "Quantifying shape transition in anisotropic plasmonic nanoparticles through geometric inversion. Application to gold bipyramids," Journal of Physics F: Metal Physics 15(14), 3914–3922 (2024).
30. N. G. Khlebtsov, "Extinction and scattering of light by nonspherical plasmonic particles in absorbing media," Journal of Quantitative Spectroscopy and Radiative Transfer 280, 108069 (2022).
31. H. Hövel, S. Fritz, A. Hilger, U. Kreibig, and M. Vollmer, "Width of cluster plasmon resonances: Bulk dielectric functions and chemical interface damping," Physical Review B 48(24), 18178–18188 (1993).
32. B. Foerster, A. Joplin, K. Kaefer, S. Celiksoy, S. Link, and C. Sönnichsen, "Chemical interface damping depends on electrons reaching the surface," ACS Nano 11(3), 2886–2893 (2017).
33. E. A. Coronado, G. C. Schatz, "Surface plasmon broadening for arbitrary shape nanoparticles: A geometrical probability approach," The Journal of Chemical Physics 119(7), 3926–3934 (2003).
34. A. Wokaun, J. P. Gordon, and P. F. Liao, "Radiation damping in surface-enhanced raman scattering," Physical Review Letters 48(14), 957–960 (1982).
35. C. Sönnichsen, T. Franzl, T. Wilk, G. Von Plessen, J. Feldmann, O. Wilson, and P. Mulvaney, "Drastic reduction of plasmon damping in gold nanorods," Physical Review Letters 88(7), 077402 (2002).
36. A. Kawabata, R. Kubo, "Electronic properties of fine metallic particles. II. Plasma resonance absorption," Journal of the Physical Society of Japan 21(9), 1765–1772 (1966).
37. A. A. Lushnikov, A. J. Simonov, "Surface plasmons in small metal particles," Zeitschrift für Physik 270(1), 17–24 (1974).
38. R. Ruppin, H. Yatom, "Size and shape effects on the broadening of the plasma resonance absorption in metals," Physica Status Solidi B Basic Research 74(2), 647–654 (1976).
39. L. Genzel, T. P. Martin, and U. Kreibig, "Dielectric function and plasma resonances of small metal particles," Zeitschrift für Physik B 21(4), 339–346 (1975).
40. H. Chen, X. Kou, Z. Yang, W. Ni, and J. Wang, "Shape- and size-dependent refractive index sensitivity of gold nanoparticles," Langmuir 24(10), 5233–5237 (2008).
41. J.-H. Lee, K. J. Gibson, G. Chen, and Y. Weizmann, "Bipyramid-templated synthesis of monodisperse anisotropic gold nanocrystals," Nature Communications 6(1), 7571 (2015).
42. D. Chateau, A. Desert, F. Lerouge, G. Landaburu, S. Santucci, and S. Parola, "Beyond the concentration limitation in the synthesis of nanobipyramids and other pentatwinned gold nanostructures," ACS Applied Materials & Interfaces Journal 11(42), 39068–39076 (2019).
43. A. Sánchez-Iglesias and M. Grzelczak, "Expanding chemical space in the synthesis of gold bipyramids," Small 21(2), 2407735 (2025).

44. A. L. Nguyen, Q. J. Griffin, A. Wang, S. Zou, and H. Jing, "Optimization of the surfactant ratio in the formation of penta-twinned seeds for precision synthesis of gold nanobipyramids with tunable plasmon resonances," The Journal of Physical Chemistry C 129(8), 4303–4312 (2025).
45. N. G. Khlebtsov, S. V. Zarkov, "Analytical models for coated plasmonic particles: Effects of shape and size-corrected dielectric function," The Journal of Chemical Physics 163(21), 214103 (2025).
46. C. Novo, D. Gomez, J. Perez-Juste, Z. Zhang, H. Petrova, M. Reismann, P. Mulvaney, and G. V. Hartland, "Contributions from radiation damping and surface scattering to the linewidth of the longitudinal plasmon band of gold nanorods: a single particle study," Physical Chemistry Chemical Physics. 8(30), 3540 (2006).
47. B. Khlebtsov, V. Khanadeev, T. Pylaev, and N. Khlebtsov, "A new T-Matrix solvable model for nanorods: tem-based ensemble simulations supported by experiments," The Journal of Physical Chemistry C 115(14), 6317–6323 (2011).
48. C. F. Bohren, D. R. Huffman, Absorption and scattering of light by small particles, Wiley, New York (1983).
49. P. Chýlek, G. Videen, D. J. W. Geldart, J. S. Dobbie, and H. C. W. Tso, "Effective medium approximations for heterogeneous particles," in Light Scattering by Nonspherical Particles: Theory, Measurements, and Applications, M. I. Mishchenko, J. W. Hovenier, and L. D. Travis (Eds.), Academic Press, San Diego (2000). ISBN 0-12-498660-9
50. J. C. Maxwell Garnett, "Colours in metal glasses and in metallic films," Philosophical Transactions of the Royal Society of London, Series A, Containing Papers of a Mathematical or Physical Character 203, 385−420 (1904).
51. D. A. G. Bruggeman, "Berechnung verschiedener physikalischer konstanten von heterogenen substanzen. I. Dielektrizitätskonstanten und leitfähigkeiten der mischkörper aus isotropen substanzen," Annalen der Physik 416(7), 636–664 (1935).
52. G. A. Niklasson, C. G. Granqvist, and O. Hunderi, "Effective medium models for the optical properties of inhomogeneous materials," Applied Optics 20(1), 26 (1981).
53. V. Ossenkopf, "Effective-medium theories for cosmic dust grains," Astronomy and Astrophysics 251, 210–219 (1991).
54. D. Stroud, F. P. Pan, "Self-consistent approach to electromagnetic wave propagation in composite media: Application to model granular metals," Physical Review B 17(4), 1602–1610 (1978).
55. P. Lalanne, W. Yan, K. Vynck, C. Sauvan, and J. Hugonin, "Light interaction with photonic and plasmonic resonances," Laser & Photonics Reviews 12(5), 1700113 (2018).
56. Q. Wang, Y. Liu, C. Li, B. Xu, S. Xu, and B. Liu, "Machine learning-enhanced nanoparticle design for precision cancer drug delivery," Advanced Science 12(30), e03138 (2025).
57. W. Al Zoubi, Y. Sheng, I. Hussain, H. Seongjun, and N. Park, "Multi-principal element nanoparticles: Synthesis strategies and machine learning prediction," Coordination Chemistry Reviews 535, 216656 (2025).
58. M. M. Saeed, E. Carthy, N. Dunne, and D. Kinahan, "Advances in nanoparticle synthesis assisted by microfluidics," Lab on a Chip 25(13), 3060–3093 (2025).
59. A. Pandian, C. Boobalan, "Ternary hybrid nanofluids: synthesis, thermal properties, machine learning insights, and emerging applications," Multiscale and Multidisciplinary Modeling, Experiments and Design 9(1), 6 (2026).
60. J.-F. Masson, J. S. Biggins, and E. Ringe, "Machine learning for nanoplasmonics," Nature Nanotechnology 18(2), 111–123 (2023).
61. A. A. Guda, M. V. Kirichkov, V. V. Shapovalov, A. I. Muravlev, D. M. Pashkov, S. A. Guda, A. P. Bagliy, S. A. Soldatov, S. V. Chapek, and A. V. Soldatov, "Machine learning analysis of reaction parameters in UV-mediated synthesis of gold nanoparticles," The Journal of Physical Chemistry C 127(2), 1097–1108 (2023).
62. A. J. Canning, J. Q. Li, J. Chen, K. Hoang, T. Thorsen, A. Vaziri, and T. Vo-Dinh, "Tunable and scalable production of nanostar particle platforms for diverse applications using an AI-integrated automated synthesis system," Journal of Materials Science 60(8), 3768–3785 (2025).